

M2DAO-Talker: Harmonizing Multi-granular Motion Decoupling and Alternating Optimization for Talking-head Generation

Kui Jiang¹, Shiyu Liu¹, Junjun Jiang¹, Xin Yang², Hongxun Yang¹, Xiaopeng Fan¹

¹Harbin Institute of Technology

²Dalian University of Technology

jiangkui@hit.edu.cn, liushiyu_aiaa@stu.hit.edu.cn

Abstract

Audio-driven talking head generation holds significant potential for film production. While existing 3D methods have advanced motion modeling and content synthesis, they often produce rendering artifacts, such as motion blur, temporal jitter, and local penetration, due to limitations in representing stable, fine-grained motion fields. Through systematic analysis, we reformulate talking head generation into a unified framework comprising three steps: video preprocessing, motion representation, and rendering reconstruction. This framework underpins our proposed M2DAO-Talker, which addresses current limitations via multi-granular motion decoupling and alternating optimization. Specifically, we devise a novel 2D portrait preprocessing pipeline to extract frame-wise deformation control conditions (motion region segmentation masks, and camera parameters) to facilitate motion representation. To ameliorate motion modeling, we elaborate a multi-granular motion decoupling strategy, which independently models non-rigid (oral and facial) and rigid (head) motions for improved reconstruction accuracy. Meanwhile, a motion consistency constraint is developed to ensure head-torso kinematic consistency, thereby mitigating penetration artifacts caused by motion aliasing. In addition, an alternating optimization strategy is designed to iteratively refine facial and oral motion parameters, enabling more realistic video generation. Experiments across multiple datasets show that M2DAO-Talker achieves state-of-the-art performance, with the 2.43 dB PSNR improvement in generation quality and 0.64 gain in user-evaluated video realism versus TalkingGaussian while with 150 FPS inference speed. Our project homepage is <https://m2dao-talker.github.io/M2DAO-Talk.github.io>

Introduction

The generation of talking head videos (Wang et al. 2024a) significantly enhances digital human realism by aligning with human perceptual expectations, making it particularly valuable for film production, immersive education platforms, and so on.

Traditional studies (Wang et al. 2023; Zhong et al. 2023; Guan et al. 2023; Zhang et al. 2023a) employ robust content generation capabilities of generative adversarial networks (GANs) for lip-sync prediction, demonstrating preliminary success in audio-driven synthesis. However, their lack of explicit motion field modeling and geometric priors leads to

limited capacity for fine-grained facial dynamics, and artifacts from fixed head pose constraints.

Recently, the 3D reconstruction area is experiencing vigorous development with deep learning technologies, such as Neural Radiance Fields (Mildenhall et al. 2021; Yang, Deng, and Zhang 2025) (NeRF) and 3D Gaussian Splatting (Kerbl et al. 2023; Fei et al. 2024) (3DGS). For talking head generation, NeRF-based methods (Guo et al. 2021; Tang et al. 2022) ameliorate structural stability through tri-plane hash encoders that compress dynamic heads into low-dimensional subspaces. While enhancing identity preservation and texture generation, these methods (Li et al. 2023; Peng et al. 2024) still face critical limitations. For example, they lack precise motion representation due to direct modeling of the relationship between position, color, and density, causing facial distortions during rapid expressions.

Addressing these issues, 3D Gaussian Splatting (3DGS) offers a promising alternative to NeRF, delivering comparable rendering quality with significantly faster inference. Recent 3DGS variants (Cho et al. 2024; Li et al. 2025) enhance temporal stability by learning explicit Gaussian fields to model motion patterns. Some approaches (Li et al. 2025) further acknowledge motion field heterogeneity across facial regions, introducing face-mouth decomposition for fine-grained motion representation. Despite improved oral rendering, three key challenges persist in 3DGS methods. First, the extraction and segmentation of motion regions via BiSeNet (Yu et al. 2018) has been prone to produce imprecise edges, resulting in blurred edges or piercing phenomena during Gaussian field modeling. Second, adopting explicit geometric priors via 3D Morphable Models (Paysan et al. 2009) (3DMM) for frame-wise head pose estimation (Li et al. 2025) causes obvious inter-frame head jitter, where the mixed effects of head pose and facial expression on 3DMM are ignored. Third, the lack of joint optimization between head and torso movement results in kinematic discontinuity and unnatural visual effect. Overall, 3DGS-based technologies (Cho et al. 2024; Li et al. 2025) lack consistency and thoroughness when decoupling motion, resulting in unnatural, warped facial repression and piercing phenomena in synthesized videos.

To circumvent these challenges, we propose M2DAO-Talker—a unified framework integrating multi-granular motion decoupling and alternating optimization for audio-

driven head-talking synthesis. Our M2DAO-Talker approach systematically organizes the task through three coordinated components: video preprocessing, motion representation, and rendering reconstruction. Preprocessing is a key step in achieving precise motion modeling. We implement a high-quality 2D talking portrait video preprocessing pipeline to achieve frame-wise extraction of deformation control parameters, motion region segmentation and camera parameters estimation. In this way, we can produce the hyperparameters of motion representation, accurate camera parameters, fine-grained semantic masks, and so on. These inputs facilitate accurate motion modeling with specific priors and significantly alleviate simulated errors.

In addition, we have developed a novel multi-granular motion decoupling scheme to bolster motion expression in M2DAO-Talker. Specifically, in addition to modeling rigid head rotation through camera parameters, we adopt the common practice of separating non-rigid head motion into facial and oral components using two dedicated branches: a Face Branch for capturing macro-scale expressions (*e.g.*, eyebrow movement, eye blinks) and an Inside Mouth Branch for modeling finer oral articulations such as phoneme-dependent tongue positions. Meanwhile, we have developed a motion consistency constraint to maintain head-to-torso kinematic consistency. Concretely, the unified representation of torso motion is learned with the Face Branch to guide more reasonable Gaussian field modeling of facial contours, producing visually pleasing and natural reconstruction results.

To achieve more coherent facial reconstruction, we introduce an alternate optimization strategy that cyclically updates parameters between the Face Branch and the Inside Mouth Branch. In this way, it encourages the network to dynamically adjust the convergence path based on the optimization errors of specific branches, enhancing physically consistent blending at facial/oral boundaries. In general, the contributions are as follows.

- We present a novel M2DAO-Talker approach for audio-driven talking head generation, which ameliorates stability and consistency of produced video by unifying multi-granular motion decoupling and alternating optimization.
- We elaborate the video preprocessing pipeline to facilitate stable and precise motion field reconstruction, which simultaneously enables frame-wise deformation control extraction, semantic motion region segmentation, and camera parameter estimation.
- We introduce the multi-granular motion decoupling scheme, an innovative solution that implements division representation of head, facial, and oral motions, cooperating with a motion consistency constraint and alternate optimization strategy to judiciously mitigate timing jitter and local penetration phenomenon.

Method

As illustrated in Figure 1, our proposed framework, **M2DAO-Talker**, synthesizes audio-driven talking-head videos from monocular portrait footage of a target speaker.

We propose a multi-granular, fully disentangled motion representation for head motion. Specifically, our 2D video preprocessing pipeline first decouples rigid **head rotation** and segments distinct facial motion regions. Using semantic masks, non-rigid motion is further decomposed into **oral movements** and **facial expressions**. Finally, a motion consistency constraint and an alternating optimization strategy are introduced to enforce coherent dynamics across motion regions. Preliminaries and details of each module follow in subsequent sections.

Preliminaries

3D Gaussian Splatting. 3D Gaussian splatting (3DGS) represents 3D information using anisotropic 3D Gaussians. Given a set of Gaussian primitives θ and camera parameters, this method computes pixel-level colors C through differentiable rendering.

Each Gaussian primitive θ is parameterized by five attributes, involving the center position $\mu \in \mathbb{R}^3$ (mean of the Gaussian distribution), the scaling factor $s \in \mathbb{R}^3$, the rotation quaternion $q \in \mathbb{R}^4$, the opacity $\alpha \in \mathbb{R}$, and the K -order spherical harmonics coefficients $SH \in \mathbb{R}^{3(k+1)(k+1)}$ for view-dependent color representation.

The distribution of the Gaussian primitive ($\theta = \{\mu, s, q, \alpha, SH\}$) is defined by its mean μ and the covariance matrix $\Sigma \in \mathbb{R}^{3 \times 3}$, depicted as

$$g(x) = \exp \left(-\frac{1}{2}(x - \mu)^T \Sigma^{-1}(x - \mu) \right), \quad (1)$$

where $\Sigma = R S S^T R^T$. Here, $S = \text{diag}(s)$ is the scaling matrix, and R is the rotation matrix derived from q .

For 2D projection, 3D Gaussians compute the projected covariance Σ' using

$$\Sigma' = J W \Sigma W^T J^T, \quad (2)$$

where W is the world-to-camera transformation matrix, and J is the Jacobian of perspective projection. Pixel colors C are rendered via alpha-blending of ordered Gaussians with

$$C = \sum_{i=1} c_i \alpha'_i \prod_{j=1}^{i-1} (1 - \alpha'_j), \quad (3)$$

where c_i denotes the view-dependent color from spherical harmonics, and α' represents the projected opacity. The total pixel opacity A is:

$$A = \sum_{i=1} \alpha'_i \prod_{j=1}^{i-1} (1 - \alpha'_j). \quad (4)$$

Video Preprocessing

We design a structured preprocessing pipeline to extract semantically disentangled motion signals from talking portrait videos, providing a clean and physically grounded foundation for subsequent deformation modeling. Our pipeline focuses on two key aspects: spatial segmentation of motion-sensitive regions and robust estimation of head pose trajectories. Details of audio-visual encoding and facial representations are deferred to the Appendix.

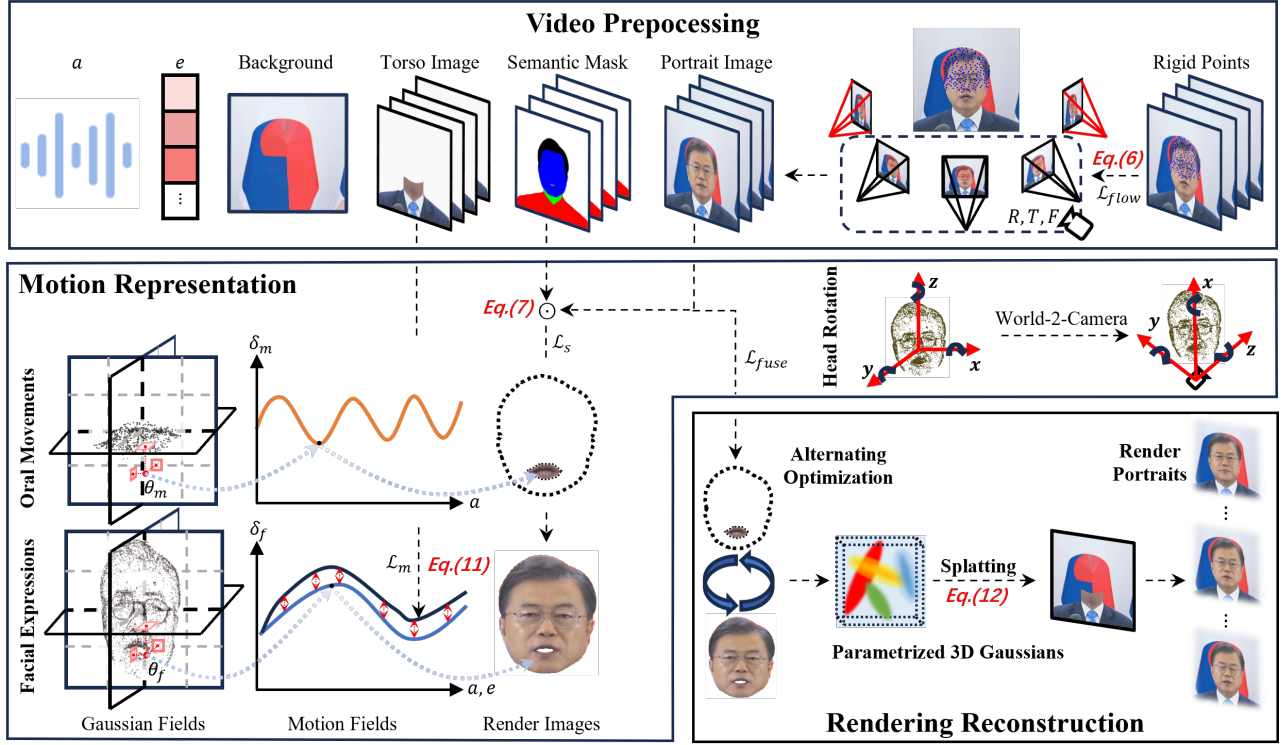


Figure 1: The M2DAO-Talker pipeline comprises three stages. i) Video Preprocessing: it extracts key features from input videos, involving portrait image I , mouth movement feature a , semantic mask M , background image I_{bg} , facial expression feature e , and camera projection parameters. ii) Motion Representation: head motion is categorized into three components: head rotation, facial expressions, and oral movements. Head rotation is parameterized using a scaling matrix T , rotation matrix R , and focal length F , while facial expressions and oral movements are modeled by two separate motion branches based on 3D Gaussian primitives. Region-specific supervision is applied to each branch using $I \odot M$ as a localized training signal, and facial deformations are regularized to maintain coherence with torso motion. iii) Rendering Reconstruction: alternating optimization cyclically updates parameters between the Face Branch and the Inside Mouth Branch, using full portrait I as ground truth.

Motion Region Segmentation (MRS). Facial motion during speech is inherently localized, driven by specific muscular activations rather than uniform deformation. To accurately model such behavior, we introduce a hybrid segmentation framework that refines the delineation of motion-relevant regions with greater granularity and robustness. Rather than relying solely on conventional facial parsing (Yu et al. 2018), we incorporate spatial priors derived from position-guided foreground extraction. Specifically, region masks are initialized based on sparse positional prompts (e.g., eyes, mouth, torso), which guide a spatial encoder (Ravi et al. 2024) to produce coherent foreground boundaries:

$$M_R = \text{Enc}_p(P_{le}, P_{re}, P_m, P_{lt}, P_{rt}), \quad (5)$$

where P_* means the key positional prompt extracted from the landmarks.

This enables more stable localization even under challenging conditions such as occlusion or background clutter. The resulting mask is then refined into semantically meaningful subregions $M_R = \{M_f, M_m\}$ through a two-stage parsing strategy. In particular, we enhance the oral region segmentation (Yu et al. 2018) by incorporating a fine-grained teeth-aware parser (Kvanchiani et al. 2023), which resolves

common edge ambiguities caused by texture homogeneity around the lips and teeth. This segmentation design serves as the basis for spatially disentangled deformation learning in later stages.

Head Pose Estimation (HPE). To model rigid motion independently of non-rigid deformations, we formulate a motion decomposition strategy (Yao et al. 2022) that yields stable camera parameters aligned with physically plausible head movement. Although prior approaches (Li et al. 2025; Cho et al. 2024) often regress pose parameters through landmark alignment, they are prone to drift due to entangled expression dynamics. In contrast, we propose to decouple rigid trajectories by identifying deformation-invariant regions across time. Specifically, we compute per-frame motion vectors and extract temporally stable keypoints (e.g., ears, hairlines) using Laplacian-filtered flow magnitude. These keypoints define a rigid motion trajectory $\{K_t\}_{t=1}^T$ that is minimally affected by facial articulation. The scaling matrix T , rotation matrix R , and focal length F of camera are then optimized by aligning projected 3D landmarks P_t with the tracked rigid trajectory:

$$\mathcal{L}_{flow} = \sum_{t=1}^T \|P_t(R_{opt}, T_{opt}, F_{opt}) - K_t\|_2. \quad (6)$$

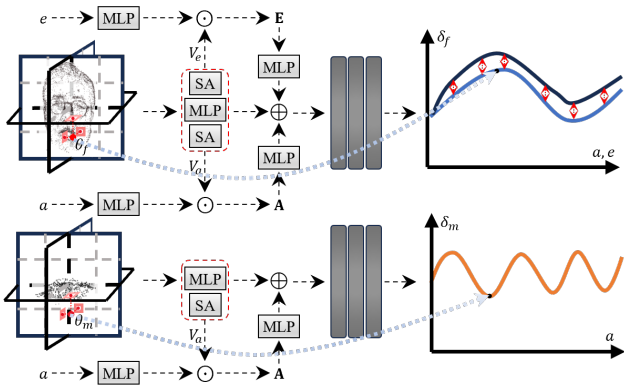


Figure 2: Detailed architecture of the network designed to capture non-rigid facial dynamics. “SA” stands for Self-Attention module.

To ensure temporal stability, frames with high flow error are filtered based on sequence-level statistics. Importantly, we preserve these frames for alternating optimization by excluding them only from the motion consistency constraint, thereby maintaining expression diversity while suppressing rigid motion noise.

Motion Representation

Our framework achieves multi-granular motion disentanglement into three distinct components: head rotation, oral movements, and facial expressions. While prior approaches attempt similar factorization, they often exhibit residual entanglement due to insufficient rigid motion modeling or inadequate semantic priors. In contrast, our method explicitly separates these motion components during preprocessing, establishing a robust foundation for downstream learning.

Specifically, we use HPE to extract rigid head rotation and MRS to localize deformable facial subregions. These steps yield high-quality initialization of semantic masks and 3D camera parameters, ensuring physically plausible alignment and precise regional control. With these decoupled signals, we deploy two dedicated deformation branches: a Face Branch for full facial expressions and an Inside Mouth Branch for internal articulations. Region masks M_f, M_m are applied during both rendering and loss computation to enforce spatial separation and prevent interference between motion types.

$$I_f = I \odot M_f, \quad I_m = I \odot M_m, \quad (7)$$

where I is the input frame and \odot denotes element-wise multiplication. We can further remove I_m and I_f from I to obtain the background image I_{bg} that contains torso motion.

As illustrated in Figure 2, we introduce an anatomically grounded attention mechanism to further decouple expressions from speech-induced dynamics. Phoneme-aware features $\mathbf{A} = \text{Enc}(a) \odot V_a$ and expression embeddings $\mathbf{E} = \text{Enc}(e) \odot V_e$ are generated via attention-guided MLPs (Guo et al. 2022), modulating localized Gaussian offsets $\delta = \{\Delta\mu, \Delta s, \Delta q\}$:

$$\delta_f = \text{MLP}(\mathcal{H}(\mu_{\text{face}}) \oplus \mathbf{A} \oplus \mathbf{E}), \quad (8)$$

$$\delta_m = \text{MLP}(\mathcal{H}(\mu_{\text{mouth}}) \oplus \mathbf{A}), \quad (9)$$

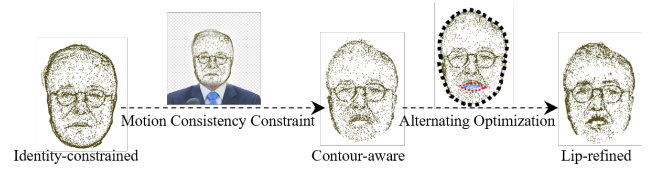


Figure 3: Iterative optimization of the facial 3DGS point cloud.

where $\mathcal{H} : \mathbb{R}^3 \rightarrow \mathbb{R}^{36}$ is a tri-plane hash encoder, and \oplus denotes feature concatenation.

Motion Consistency Constraint (MCC). To further promote biomechanical coherence, we introduce a motion-level constraint that aligns facial deformations with global torso dynamics. This is implemented through a novel *full-portrait supervision* strategy applied during dynamic refinement.

Following standard practice for static initialization, both branches first reconstruct region-specific appearance using pixel-wise ℓ_1 and structural DSSIM losses:

$$\mathcal{L}_s(\hat{I}_r, I_r) = \ell_1(\hat{I}_r, I_r) + \lambda \mathcal{L}_{\text{SSIM}}(\hat{I}_r, I_r), \quad (10)$$

where $\hat{I}_r = \{\hat{I}_f, \hat{I}_m\}$ denotes predicted region images and $I_r = \{I_f, I_m\}$ denotes ground-truth.

Our core innovation lies in the dynamic learning, where we introduce full-portrait supervision by compositing facial renderings with background using facial transparency A_f : $\hat{I}_{bg} = \hat{I}_f \times A_f + I_{bg} \times (1 - A_f)$. This enables global optimization through combined objectives:

$$\mathcal{L}_m = \mathcal{L}_s(\hat{I}_{bg}, I) + \gamma \mathcal{L}_{\text{LPIPS}}(\hat{I}_{bg}, I). \quad (11)$$

Unlike prior work constrained to facial regions, this novel supervision strategy explicitly couples facial motion with torso dynamics. However, for the Inside Mouth Branch, we still adopt specific region constraints for optimization.

This formulation enforces harmonious deformation between facial regions (especially the audio-responsive lower face) and adjacent torso motion. By simultaneously optimizing the transparency parameter α for each 3D Gaussian, we generate temporally consistent alpha mattes that preserve boundary details during face-torso transitions. As shown in Figure 3, this constraint sharpens point cloud contours along face-torso interface, improving motion stability and anatomical coherence without architectural overhead.

Alternating Optimization Reconstruction

Synthesizing photorealistic talking heads from disentangled motion sources requires coordinated facial and intra-oral rendering. However, joint optimization under motion consistency constraints often introduces boundary artifacts like lip color leakage and tooth discoloration. We attribute these to imbalanced supervision: i) the facial mask M_f typically excludes inner-lip regions; ii) under-constrained color reconstruction in the Face Branch; iii) compensatory overfitting in the Inside Mouth Branch, resulting in unnatural shading and misalignment.

Alternating Optimization Strategy. To address this, we implement a decoupled, two-branch approach. We firstly optimize the Face Branch while freezing the Inside Mouth

Methods	Rendering Quality			Motion Quality			Efficiency	
	PSNR \uparrow	LPIPS \downarrow	SSIM \uparrow	LMD \downarrow	AUE-(L/U) \downarrow	Sync-C \uparrow	Time	FPS
NeRF	AD-NeRF (Guo et al. 2021)	30.07	0.1042	0.9689	2.998	1.01/0.97	6.053	18.7h 0.11
	RAD-NeRF (Tang et al. 2022)	31.21	0.0643	0.9733	2.961	0.95/0.83	5.726	5.3h 28.7
	ER-NeRF (Li et al. 2023)	31.66	0.0385	0.9732	2.745	0.76/0.64	6.633	2.1h 31.2
	SyncTalk (Peng et al. 2024)	<u>33.90</u>	<u>0.0246</u>	<u>0.9950</u>	<u>2.685</u>	<u>0.67/0.32</u>	<u>7.672</u>	2.0h 52
3DGS	GaussianTalker (Cho et al. 2024)	31.75	0.0494	0.9942	2.805	0.83/0.70	6.37	3.2h 95
	TalkingGaussian (Li et al. 2025)	32.04	0.0319	0.9947	2.714	0.70/0.32	6.284	0.5h 108
	M2DAO-Talker (Ours)	34.47	0.0229	0.9967	2.636	0.61/0.26	7.756	<u>0.6h</u> 150

Table 1: Quantitative results of Self-Reconstruction. We emphasize the highest and second-highest results by bolding and underlining the corresponding values, respectively.

Branch, allowing stable estimation of coarse facial geometry and appearance, especially around the lip region. Then we jointly fine-tune both branches: enhancing color/opacity of the mouth region and refining facial outputs, enabling collaborative correction of previous approximations while avoiding destructive interference. This alternating optimization improves convergence, harmonizes overlapping regions, and maintains motion consistency. As shown in Figure 3, it yields smoother point cloud geometry and enhanced appearance at facial-oral boundaries.

Given deformation parameters (δ_f , δ_m), Gaussian primitive (θ_f , θ_m) and camera parameters, we synthesize the final image through:

$$\hat{I}_{\text{fuse}} = \hat{I}_f \times A_f + (\hat{I}_m \times A_m + I_{\text{bg}} \times (1 - A_m)) \times (1 - A_f), \quad (12)$$

and supervise it using the following reconstruction loss:

$$\mathcal{L}_{\text{fuse}} = \mathcal{L}_s(\hat{I}_{\text{fuse}}, I) + \gamma \mathcal{L}_{\text{LPIPS}}(\hat{I}_{\text{fuse}}, I). \quad (13)$$

Experiments

Experimental Settings

Dataset. Following prior works (Ye et al. 2023; Li et al. 2023; Guo et al. 2021; Tang et al. 2022), we use seven publicly available video clips to train and evaluate both our M2DAO-Talker and baselines. Each video averages 7,066 frames at 25 FPS, focusing on a centered portrait, which are 512 \times 512 (“Obama2”, “May”, “Shaheen” and “Lieu”) or 450 \times 450 (“Obama”, “Jae-in”, and “Obama1”) resolution.

Comparison Baseline. We provide comprehensive comparison and analysis against several state-of-the-art 2D generative models (IP-LAP (Zhong et al. 2023), TalkLip (Wang et al. 2023) and DINet (Zhang et al. 2023b)), NeRF-based approaches (AD-NeRF (Guo et al. 2021), RAD-NeRF (Tang et al. 2022), ER-NeRF (Li et al. 2023) and SyncTalk (Peng et al. 2024)) and 3DGS-based methods (GaussianTalker (Cho et al. 2024) and TalkingGaussian (Li et al. 2025)).

Evaluation Metrics. For static image quality, we report Peak Signal-to-Noise Ratio (PSNR), Structural Similarity Index (SSIM) (Wang et al. 2004), and Learned Perceptual Image Patch Similarity (LPIPS) (Zhang et al. 2018) to assess overall reconstruction accuracy, structural integrity, and high-frequency detail preservation, respectively. For dynamic motion evaluation, we employ SyncNet (Chung and

Methods		Motion Quality		
		LMD ↓	AUE-(L/U) ↓	Sync-C ↑
GAN	IP-LAP (Zhong et al. 2023)	3.266	1.01/-	7.047
	DINet (Zhang et al. 2023b)	3.366	1.18/-	7.645
	TalkLip (Wang et al. 2023)	3.376	1.01/-	6.536
	M2DAO-Talker (Ours)	2.636	0.61/0.26	7.756

Table 2: Comparison results of Self-Reconstruction with GAN-based methods. The best results are indicated in bold.

Zisserman 2017) to measure lip-sync quality via Landmark Distance (LMD), Confidence Score (Sync-C), and Error Distance (Sync-D). To further quantify facial expressiveness, we report Upper-face and Lower-face AU errors (AUE-U / AUE-L) to assess the precision of facial motion in different regions like TalkingGaussian (Li et al. 2025).

Implementation Details. We adopt a two-phase training scheme per identity: 50K iterations of joint training for both branches, followed by 20K iterations of alternating optimization. The network is trained using Adam and AdamW with a learning rate of 5×10^{-4} . In the loss functions (Equations (10), (11) and (13)), we set $\lambda = 0.2$ and $\gamma = 0.5$. All experiments are conducted on NVIDIA RTX 3090 GPUs.

Comparison with SOTA

Comparison Settings. In our quantitative evaluation, we assess the proposed method under two distinct conditions: the *self-reconstruction setting* and the *lip synchronization setting*. In the self-reconstruction setting, a 10-to-1 train-validation split is applied to each dataset to evaluate reconstruction fidelity. For the lip synchronization setting, we perform cross-domain evaluation using audio from unseen speakers (“Lieu” and “Shaheen”) to drive target identities (“Obama” and “May”), including cross-gender cases, to test generalization and synchronization robustness.

Quantitative Results. Our method surpasses existing approaches in most metrics (Tables 1 and 2). M2DAO-Talker achieves the highest PSNR of **34.47** and lowest LPIPS of **0.0229**, outperforming SyncTalk (33.90) and TalkingGaussian (32.04) by leveraging improved preprocessing and region-specific deformation. In motion accuracy, it achieves an LMD of **2.636** and AUE-L of **0.61**, indicating effective motion disentanglement. Moreover, a Sync-C of **7.756** exceeds even specialized 2D lip-sync baselines, thanks to our

Method	“Shaheen” Audio				“Lieu” Audio			
	“Obama”		“May”		“Obama”		“May”	
	Sync-D ↓	Sync-C ↑	Sync-D ↓	Sync-C ↑	Sync-D ↓	Sync-C ↑	Sync-D ↓	Sync-C ↑
DINet (Zhang et al. 2023b)	8.606	<u>7.481</u>	8.201	<u>7.295</u>	8.450	6.851	8.226	6.470
IP-LAP (Zhong et al. 2023)	9.190	<u>6.135</u>	9.819	<u>5.316</u>	10.175	4.316	9.392	5.077
TalkLip (Wang et al. 2023)	10.967	4.754	9.553	5.488	11.648	3.459	11.679	3.151
RAD-NeRF (Tang et al. 2022)	8.633	7.166	12.012	3.054	9.051	6.163	12.044	2.449
ER-NeRF (Li et al. 2023)	8.240	7.628	9.775	5.529	8.103	7.179	10.017	4.782
SyncTalk (Peng et al. 2024)	8.600	7.099	8.903	6.350	8.903	6.350	<u>7.508</u>	<u>7.780</u>
GaussianTalker (Cho et al. 2024)	9.415	6.686	8.926	6.576	10.171	5.441	10.943	4.198
TalkingGaussian (Li et al. 2025)	10.596	4.543	11.450	3.179	9.702	5.746	9.849	5.039
M2DAO-Talker (Ours)	<u>8.486</u>	7.255	7.667	8.111	<u>8.371</u>	<u>6.916</u>	7.028	8.333

Table 3: Quantitative results of cross-domain audio-driven Lip Synchronization.



Figure 4: Qualitative results of Image Quality Comparison. Our method effectively eliminates edge blur and corrects facial distortions, blinking errors, and unnatural head-torso synthesis that were present in previous approaches. For improved visualization, please zoom in.

alternating optimization strategy. In cross-domain lip synchronization (Table 3), our method demonstrates stable and consistent performance across identities and genders. Particularly in “Lieu” to “May”, it maintains accurate synchronization despite large speaker variation, highlighting its ability to generalize phoneme-to-motion mapping independently of identity. While ER-NeRF performs well in certain scenarios, it fluctuates significantly due to its direct audio-to-lip mapping, which lacks robustness to identity shifts. In contrast, M2DAO-Talker’s multi-granular motion modeling ensures reliable identity-consistent synthesis across diverse speaker conditions.

Image Quality Comparison. Figure 4 visually compares self-reconstruction results from SyncTalk, TalkingGaussian, and our method. Our approach achieves superior facial detail sharpness and cleaner head-background boundaries. SyncTalk exhibits facial distortions (gray boxes/red arrows)

due to inadequate motion field modeling, particularly misarticulating lip and eye regions. Our motion disentanglement resolves these limitations. TalkingGaussian shows head-torso kinematic discontinuity (yellow box) and blending artifacts from poor segmentation (yellow arrows). Our Motion Consistency Constraint (MCC) eliminates discontinuity while hybrid segmentation ensures precise mask boundaries and artifact-free foreground-background fusion.

User Study. To evaluate perceptual quality, we conduct a user study with 20 participants rating 49 half-minute videos from six models and Ground Truth. Each subject scores seven videos (1–5 scale) on the video realness, image quality and lip-sync accuracy. As shown in Figure 5, our M2DAO-Talker achieves the highest overall ratings across all criteria, reaching 87% of GT scores on average and the lowest lip-sync error (0.49). These results highlight the perceptual advantages of our motion disentanglement and alternating

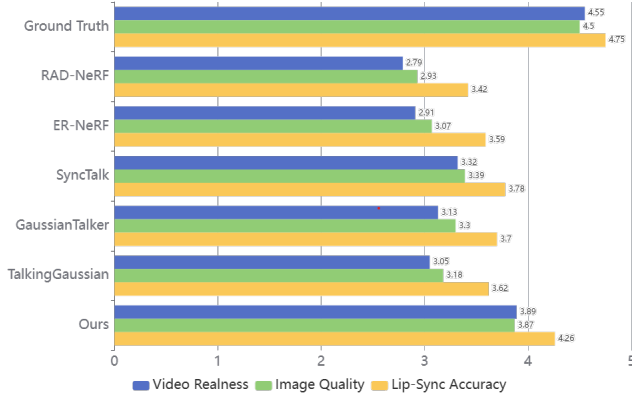


Figure 5: User Study. The rating is in the range of 1-5, higher denotes better performance.

optimization design.

Ablation Study

Ablation Setting. To assess the contribution of each module, we conduct ablation studies on key components across our framework. For MRS and HPE, which involve specific backbone design choices, we evaluate by replacing them with widely adopted alternatives under controlled settings. Specifically, we substitute MRS with BiseNet (Yu et al. 2018) and conduct experiments on datasets such as “Jaemin”, “Shaheen”, and “May” where boundary ambiguity is prominent. For HPE, we revert to 3DMM-based camera estimation and replace other methods’ estimations with HPE. We evaluate the results on the “Obama”, “Obama1”, and “Obama2” sequences, which feature diverse head movements. In contrast, we ablate AOS and MCC on all seven datasets to comprehensively assess the global impact.

Ablation Results. Replacing the standard segmentation backbone with MRS yields consistent improvements (Table 4). These gains stem from MRS’s precise boundary localization, which reduces motion interference and enables more accurate region-specific deformation. Even SyncTalk, which lacks explicit deformation modeling, benefits from MRS, confirming its general utility for motion-aware synthesis. Incorporating HPE also improves all metrics (Table 5), as it explicitly decouples rigid head rotation from facial dynamics, enabling smoother and more stable deformation learning, especially under large pose variations. With HPE, the attention maps of upper-face (V_e) and lower-face (V_a) focus more on the corresponding regions (Figure 6), indicating that accurate decoupling of rigid head rotation enhances the learning of non-rigid facial motion.

Backbone	MRS	BN	PSNR \uparrow	LPIPS \downarrow	LMD \downarrow
M2DAO-Talker (Ours)	\checkmark		35.041	0.0223	2.4575
		\checkmark	34.400	0.0243	2.4586
TalkingGaussian (Li et al. 2025)	\checkmark		31.519	0.0360	2.5973
		\checkmark	33.260	0.0291	2.5603
SyncTalk (Peng et al. 2024)	\checkmark		33.955	0.0249	2.5374
		\checkmark	34.355	0.0261	2.5733

Table 4: MRS ablation result.

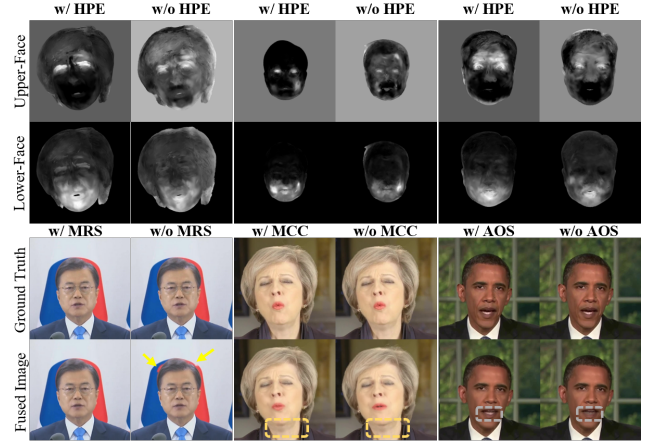


Figure 6: Visualization of region attention map and reconstruction result in individual components ablation.

Disabling MCC results in poor quality (Table 6) and inconsistency in motion, where face and torso move incoherently, leading to artifacts such as jagged contours and depth violations (Figure 6). These results highlight MCC’s importance in enforcing biomechanical coherence by aligning facial motion with torso dynamics. Replacing AOS with naive joint training causes color bleeding and perceptual degradation around the lips (Table 6). The lack of staged supervision leads to early overfitting in the Inside Mouth Branch, reducing lip detail fidelity and disrupting facial-oral continuity.

Backbone	HPE	PSNR \uparrow	LPIPS \downarrow	LMD \downarrow
M2DAO-Talker (Ours)	\checkmark	33.746	0.0249	2.809
		33.648	0.0249	2.799
TalkingGaussian (Li et al. 2025)		32.384	0.0294	2.825
	\checkmark	33.215	0.0265	2.762
SyncTalk (Peng et al. 2024)		33.439	0.0260	2.839
	\checkmark	33.669	0.0260	2.787

Table 5: HPE ablation result.

Backbone	MCC	AOS	PSNR \uparrow	LPIPS \downarrow	LMD \downarrow
M2DAO-Talker (Ours)	\checkmark	\checkmark	34.475	0.0229	2.636
		\checkmark	34.123	0.0239	2.624
	\checkmark		34.375	0.0229	2.620

Table 6: MCC and AOS ablation result.

Conclusion

We propose **M2DAO-Talker**, a novel audio-driven talking head framework that improves video stability and coherence through multi-granular motion disentanglement and alternating optimization. A robust 2D video preprocessing pipeline is developed to extract frame-wise deformation control, segment semantic motion regions, and estimate camera parameters. By decoupling head motion into rigid, facial, and oral components, and reinforcing coherence via a motion consistency constraint and alternating optimization, our approach effectively reduces timing jitter and artifacts, achieving high-quality, real-time synthesis.

References

- Afouras, T.; Chung, J. S.; Senior, A.; Vinyals, O.; and Zisserman, A. 2018. Deep audio-visual speech recognition. *IEEE Transactions on Pattern Analysis and Machine Intelligence*, 44(12): 8717–8727.
- Baltrusaitis, T.; Zadeh, A.; Lim, Y. C.; and Morency, L.-P. 2018. OpenFace 2.0: Facial Behavior Analysis Toolkit. In *International Conference on Automatic Face and Gesture Recognition*, 59–66. IEEE.
- Brox, T.; Bruhn, A.; Papenberger, N.; and Weickert, J. 2004. High accuracy optical flow estimation based on a theory for warping. In *European Conference on Computer Vision*, 25–36. Springer.
- Cho, K.; Lee, J.; Yoon, H.; Hong, Y.; Ko, J.; Ahn, S.; and Kim, S. 2024. GaussianTalker: Real-Time High-Fidelity Talking Head Synthesis with Audio-Driven 3D Gaussian Splatting. In *ACM International Conference on Multimedia*, 10985–10994.
- Chung, J. S.; and Zisserman, A. 2017. Lip reading in the wild. In *Asian Conference on Computer Vision*, 87–103. Springer.
- Dosovitskiy, A.; Fischer, P.; Ilg, E.; Hausser, P.; Hazirbas, C.; Golkov, V.; Van Der Smagt, P.; Cremers, D.; and Brox, T. 2015. FlowNet: Learning optical flow with convolutional networks. In *IEEE/CVF International Conference on Computer Vision*, 2758–2766.
- Duan, Y.; Wei, F.; Dai, Q.; He, Y.; Chen, W.; and Chen, B. 2024. 4d-rotor gaussian splatting: towards efficient novel view synthesis for dynamic scenes. In *ACM SIGGRAPH 2024 Conference Papers*, 1–11.
- Ekman, P.; and Friesen, W. V. 1978. Facial action coding system. *Environmental Psychology & Nonverbal Behavior*.
- Fei, B.; Xu, J.; Zhang, R.; Zhou, Q.; Yang, W.; and He, Y. 2024. 3D Gaussian Splatting as New Era: A Survey. *IEEE Transactions on Visualization and Computer Graphics*, (01): 1–20.
- Guan, J.; Zhang, Z.; Zhou, H.; Hu, T.; Wang, K.; He, D.; Feng, H.; Liu, J.; Ding, E.; Liu, Z.; et al. 2023. Stylesync: High-fidelity generalized and personalized lip sync in style-based generator. In *IEEE/CVF Conference on Computer Vision and Pattern Recognition*, 1505–1515.
- Guo, M.-H.; Liu, Z.-N.; Mu, T.-J.; and Hu, S.-M. 2022. Beyond self-attention: External attention using two linear layers for visual tasks. *IEEE Transactions on Pattern Analysis and Machine Intelligence*, 45(5): 5436–5447.
- Guo, Y.; Chen, K.; Liang, S.; Liu, Y.-J.; Bao, H.; and Zhang, J. 2021. Ad-nerf: Audio driven neural radiance fields for talking head synthesis. In *IEEE/CVF International Conference on Computer Vision*, 5784–5794.
- Horn, B. K.; and Schunck, B. G. 1981. Determining optical flow. *Artificial Intelligence*, 17(1-3): 185–203.
- Hu, L.; Zhang, H.; Zhang, Y.; Zhou, B.; Liu, B.; Zhang, S.; and Nie, L. 2024. Gaussianavatar: Towards realistic human avatar modeling from a single video via animatable 3d gaussians. In *IEEE/CVF Conference on Computer Vision and Pattern Recognition*, 634–644.
- Huang, N.; Wei, X.; Zheng, W.; An, P.; Lu, M.; Zhan, W.; Tomizuka, M.; Keutzer, K.; and Zhang, S. 2024. S^3 Gaussian: Self-Supervised Street Gaussians for Autonomous Driving. *arXiv preprint arXiv:2405.20323*.
- Huang, Z.; Shi, X.; Zhang, C.; Wang, Q.; Cheung, K. C.; Qin, H.; Dai, J.; and Li, H. 2022. Flowformer: A transformer architecture for optical flow. In *European Conference on Computer Vision*, 668–685. Springer.
- Kerbl, B.; Kopanas, G.; Leimkühler, T.; and Drettakis, G. 2023. 3d gaussian splatting for real-time radiance field rendering. *ACM Transactions on Graphics*, 42(4).
- Kvanchiani, K.; Petrova, E.; Efremyan, K.; Sautin, A.; and Kapitanov, A. 2023. EasyPortrait–Face Parsing and Portrait Segmentation Dataset.
- Li, J.; Zhang, J.; Bai, X.; Zheng, J.; Ning, X.; Zhou, J.; and Gu, L. 2025. Talkinggaussian: Structure-persistent 3d talking head synthesis via gaussian splatting. In *European Conference on Computer Vision*, 127–145.
- Li, J.; Zhang, J.; Bai, X.; Zhou, J.; and Gu, L. 2023. Efficient region-aware neural radiance fields for high-fidelity talking portrait synthesis. In *IEEE/CVF International Conference on Computer Vision*, 7568–7578.
- Liu, S.; and Hao, J. 2023. Generating Talking Face With Controllable Eye Movements by Disentangled Blinking Feature. *IEEE Transactions on Visualization and Computer Graphics*, 29(12): 5050–5061.
- Lu, Y.; Chai, J.; and Cao, X. 2021. Live speech portraits: real-time photorealistic talking-head animation. *ACM Transactions on Graphics*, 40(6): 1–17.
- Mémin, E.; and Pérez, P. 1998. Dense estimation and object-based segmentation of the optical flow with robust techniques. *IEEE Transactions on Image Processing*, 7(5): 703–719.
- Mildenhall, B.; Srinivasan, P. P.; Tancik, M.; Barron, J. T.; Ramamoorthi, R.; and Ng, R. 2021. Nerf: Representing scenes as neural radiance fields for view synthesis. *Communications of the ACM*, 65(1): 99–106.
- Park, K.; Sinha, U.; Barron, J. T.; Bouaziz, S.; Goldman, D. B.; Seitz, S. M.; and Martin-Brualla, R. 2021a. Nerfies: Deformable neural radiance fields. In *IEEE/CVF International Conference on Computer Vision*, 5865–5874.
- Park, K.; Sinha, U.; Hedman, P.; Barron, J. T.; Bouaziz, S.; Goldman, D. B.; Martin-Brualla, R.; and Seitz, S. M. 2021b. HyperNeRF: a higher-dimensional representation for topologically varying neural radiance fields. *ACM Transactions on Graphics (TOG)*, 40(6): 1–12.
- Paysan, P.; Knothe, R.; Amberg, B.; Romdhani, S.; and Vetter, T. 2009. A 3D face model for pose and illumination invariant face recognition. In *IEEE International Conference on Advanced Video and Signal based Surveillance*, 296–301. IEEE.
- Peng, Z.; Hu, W.; Shi, Y.; Zhu, X.; Zhang, X.; Zhao, H.; He, J.; Liu, H.; and Fan, Z. 2024. SyncTalk: The devil is in the synchronization for talking head synthesis. In *IEEE/CVF Conference on Computer Vision and Pattern Recognition*, 666–676.

- Prajwal, K.; Mukhopadhyay, R.; Namboodiri, V. P.; and Jawahar, C. 2020. A lip sync expert is all you need for speech to lip generation in the wild. In *ACM International Conference on Multimedia*, 484–492.
- Pumarola, A.; Corona, E.; Pons-Moll, G.; and Moreno-Noguer, F. 2021. D-nerf: Neural radiance fields for dynamic scenes. In *IEEE/CVF Conference on Computer Vision and Pattern Recognition*, 10318–10327.
- Ravi, N.; Gabeur, V.; Hu, Y.-T.; Hu, R.; Ryali, C.; Ma, T.; Khedr, H.; Rädle, R.; Rolland, C.; Gustafson, L.; et al. 2024. Sam 2: Segment anything in images and videos. *arXiv preprint arXiv:2408.00714*.
- Sun, S.; Chen, Y.; Zhu, Y.; Guo, G.; and Li, G. 2022a. Sk-flow: Learning optical flow with super kernels. *Advances in Neural Information Processing Systems*, 35: 11313–11326.
- Sun, Y.; Zhou, H.; Wang, K.; Wu, Q.; Hong, Z.; Liu, J.; Ding, E.; Wang, J.; Liu, Z.; and Hideki, K. 2022b. Masked lip-sync prediction by audio-visual contextual exploitation in transformers. In *SIGGRAPH Asia 2022 Conference Papers*, 1–9.
- Tang, J.; Wang, K.; Zhou, H.; Chen, X.; He, D.; Hu, T.; Liu, J.; Zeng, G.; and Wang, J. 2022. Real-time neural radiance talking portrait synthesis via audio-spatial decomposition. *arXiv preprint arXiv:2211.12368*.
- Teed, Z.; and Deng, J. 2020. Raft: Recurrent all-pairs field transforms for optical flow. In *European Conference on Computer Vision*, 402–419. Springer.
- Tretschk, E.; Tewari, A.; Golyanik, V.; Zollhöfer, M.; Lassner, C.; and Theobalt, C. 2021. Non-rigid neural radiance fields: Reconstruction and novel view synthesis of a dynamic scene from monocular video. In *IEEE/CVF International Conference on Computer Vision*, 12959–12970.
- Wang, J.; Qian, X.; Zhang, M.; Tan, R. T.; and Li, H. 2023. Seeing what you said: Talking face generation guided by a lip reading expert. In *IEEE/CVF Conference on Computer Vision and Pattern Recognition*, 14653–14662.
- Wang, M.; Zhao, S.; Dong, X.; and Shen, J. 2024a. High-Fidelity and High-Efficiency Talking Portrait Synthesis With Detail-Aware Neural Radiance Fields. *IEEE Transactions on Visualization and Computer Graphics*, (01): 1–14.
- Wang, Q.; Ye, V.; Gao, H.; Austin, J.; Li, Z.; and Kanazawa, A. 2024b. Shape of motion: 4d reconstruction from a single video. *arXiv preprint arXiv:2407.13764*.
- Wang, S.; Li, L.; Ding, Y.; Fan, C.; and Yu, X. 2021. Audio2head: Audio-driven one-shot talking-head generation with natural head motion. In *International Joint Conference on Artificial Intelligence*, 1098–1105.
- Wang, Z.; Bovik, A. C.; Sheikh, H. R.; and Simoncelli, E. P. 2004. Image quality assessment: from error visibility to structural similarity. *IEEE Transactions on Image Processing*, 13(4): 600–612.
- Wedel, A.; Cremers, D.; Pock, T.; and Bischof, H. 2009. Structure-and motion-adaptive regularization for high accuracy optic flow. In *IEEE/CVF International Conference on Computer Vision*, 1663–1668. IEEE.
- Wu, G.; Yi, T.; Fang, J.; Xie, L.; Zhang, X.; Wei, W.; Liu, W.; Tian, Q.; and Wang, X. 2024. 4d gaussian splatting for real-time dynamic scene rendering. In *IEEE/CVF Conference on Computer Vision and Pattern Recognition*, 20310–20320.
- Yang, L.; Deng, B.; and Zhang, J. 2025. Scalable and high-quality neural implicit representation for 3D reconstruction. *IEEE Transactions on Visualization & Computer Graphics*.
- Yang, Z.; Gao, X.; Zhou, W.; Jiao, S.; Zhang, Y.; and Jin, X. 2024a. Deformable 3d gaussians for high-fidelity monocular dynamic scene reconstruction. In *IEEE/CVF Conference on Computer Vision and Pattern Recognition*, 20331–20341.
- Yang, Z.; Yang, H.; Pan, Z.; and Zhang, L. 2024b. Real-time Photorealistic Dynamic Scene Representation and Rendering with 4D Gaussian Splatting. In *International Conference on Learning Representations (ICLR)*.
- Yao, S.; Zhong, R.; Yan, Y.; Zhai, G.; and Yang, X. 2022. Dfa-nerf: Personalized talking head generation via disentangled face attributes neural rendering. *arXiv preprint arXiv:2201.00791*.
- Ye, Z.; Jiang, Z.; Ren, Y.; Liu, J.; He, J.; and Zhao, Z. 2023. GeneFace: Generalized and High-Fidelity Audio-Driven 3D Talking Face Synthesis.
- Yu, C.; Wang, J.; Peng, C.; Gao, C.; Yu, G.; and Sang, N. 2018. Bisenet: Bilateral segmentation network for real-time semantic segmentation. In *European Conference on Computer Vision*, 325–341.
- Zhang, C.; Ni, S.; Fan, Z.; Li, H.; Zeng, M.; Budagavi, M.; and Guo, X. 2023a. 3D Talking Face With Personalized Pose Dynamics. *IEEE Transactions on Visualization and Computer Graphics*, 29(2): 1438–1449.
- Zhang, R.; Isola, P.; Efros, A. A.; Shechtman, E.; and Wang, O. 2018. The unreasonable effectiveness of deep features as a perceptual metric. In *IEEE/CVF Conference on Computer Vision and Pattern Recognition*, 586–595.
- Zhang, Z.; Hu, Z.; Deng, W.; Fan, C.; Lv, T.; and Ding, Y. 2023b. Dinet: Deformation inpainting network for realistic face visually dubbing on high resolution video. In *AAAI Conference on Artificial Intelligence*, 3543–3551.
- Zhong, W.; Fang, C.; Cai, Y.; Wei, P.; Zhao, G.; Lin, L.; and Li, G. 2023. Identity-preserving talking face generation with landmark and appearance priors. In *IEEE/CVF Conference on Computer Vision and Pattern Recognition*, 9729–9738.
- Zhuang, Y.; Cheng, B.; Cheng, Y.; Jin, Y.; Liu, R.; Li, C.; Cheng, X.; Liao, J.; and Lin, J. 2024. Learn2Talk: 3D Talking Face Learns from 2D Talking Face. *IEEE Transactions on Visualization and Computer Graphics*, 1–13.

Appendix:M2DAO-Talker

This appendix provides additional materials that complement the main text. First, we include a dedicated **Related Works** section to review prior studies closely related to our auxiliary modules and ablation design, which were not discussed in the main paper to maintain focus and brevity. Next, we elaborate on two supporting modules used during pre-processing—namely, the *Facial Action Encoder* and *Audio-Visual Encoder*—which play a critical role in extracting semantically meaningful motion cues but are not covered in the main pipeline description. Finally, we present ablation experiments to systematically evaluate the individual contributions of these components to the final reconstruction quality and motion accuracy.

Related Works

In this section, we briefly review the more recent advances in the field of talking head synthesis and motion field modeling.

Talking Head Synthesis

Audio-driven talking head generation aims at generating videos with accurate lip movements and realistic facial animations based on input audio. Early methods, primarily based on 2D GANs (Wang et al. 2023; Zhang et al. 2023b; Zhong et al. 2023; Guan et al. 2023; Sun et al. 2022b; Prajwal et al. 2020), have achieved considerable progress in terms of photorealism. However, only the lip regions are reconstructed (Prajwal et al. 2020), which neglects other facial movements, facial expressions in particular. Further, some efforts propose to learn the complete facial representation (Lu, Chai, and Cao 2021; Wang et al. 2021), but only display a fixed head posture due to the absence of a 3D geometric modeling.

Compared to CNN-based technologies, NeRF (Mildenhall et al. 2021) shows impressive capability for continuous volumetric scene representation, which has garnered attention in employing for audio-driven talking head generation. For example, AD-NeRF (Guo et al. 2021) proposes to project audio features to dynamic neural radiance fields, enabling portrait rendering by decoupling head and torso motion. To optimize modeling efficiency, researchers introduce the multi-resolution hash (Tang et al. 2022) to encode spatial and audio information independently while decomposing the 3D motion field into three-plane hash representation to minimize collisions (Li et al. 2023). Meanwhile, SyncTalk (Peng et al. 2024) emphasizes synchronization as a key challenge, and introduces an Audio-Visual Encoder for better audio-visual alignment.

Despite significant advancements, NeRF-based methods learn implicit relationships among position, color, and density, which inevitably suffer from facial distortion and unnatural deformation due to the absence of geometrical constraints. Compared to NeRF, 3DGS utilizes the explicit geometry information to model scene, which shows faster and

more efficient rendering while preserving fine details. More recently, 3DGS has been employed for audio-driven talking head generation (Zhuang et al. 2024; Cho et al. 2024; Li et al. 2025). For example, GaussianTalker (Cho et al. 2024) proposes to learn mutual refinement of spatial-audio information, and characterizes motion field to improve facial fidelity and lip synchronization. Building on this, Talking-Gaussian (Li et al. 2025) decouples oral movements and facial expressions to achieve finer grained motion representation, while using incremental sampling methods to improve compatibility between 3DGS and deformation.

However, these approaches still face challenges, including edge ambiguities in semantic masks, incomplete decoupling of head motion and inconsistency between torso and facial motion. To address these issues, we introduce 2D segmentation priors to refine semantic parsing and head motion priors to optimize head pose estimation. Meanwhile, we learn the head-torso unified representation to maintain motion consistency, enhancing the quality of the generated video.

Motion Field Modeling

Prior to deep learning, previous methods (Horn and Schunck 1981; Wedel et al. 2009; Mémin and Pérez 1998; Brox et al. 2004) focus on object-wise motion modeling, and estimate pixel-wise motion vectors using brightness constancy constraints. And then researchers introduce CNNs to regress motion vectors via an encoder-decoder structure (Dosovitskiy et al. 2015; Teed and Deng 2020; Huang et al. 2022; Sun et al. 2022a).

However, 2D motion field-based models struggle with precise motion representation due to a lack of scene information constraints, leading to unnatural deformations under occlusion or viewpoint changes. NeRF-based approaches consider both geometric shapes and motion states, and learn the relationships among position, color, and density for 3D reconstruction of complex scenes (Park et al. 2021a; Pumarola et al. 2021; Park et al. 2021b; Tretschk et al. 2021). For instance, D-NeRF (Pumarola et al. 2021) uses a deformation network to project motion field coordinates to a NeRF-based canonical space, while Nerfies (Park et al. 2021a) correlates the motion fields with latent codes to model intricate scenarios, such as human motion. While gaining impressive rendering quality, due to the lack of explicit geometric constraints, these methods produce unsatisfied results with obvious motion distortions in the case of rapid movements. By explicitly regulating spatial point variations through motion field representation, 3DGS effectively models temporal changes in dynamic scenes (Wu et al. 2024; Duan et al. 2024; Hu et al. 2024; Yang et al. 2024b,a; Wang et al. 2024b; Huang et al. 2024).

However, existing 3DGS-based approaches primarily derive motion dynamics function from temporal sequences, where deformation fields are conditioned solely on frame indices or timestamps. Previous works reveal that nonverbal facial actions introduce motion variances uncorrelated with

phoneme timing and features alter articulation dynamics beyond temporal alignment. It indicates that audio-driven motions are governed with multiple factors where time serves merely as a carrier variable. To bridge this gap, we extract phoneme-aligned mouth movements features and person-agnostic facial expression features from 2D video as control conditions. And we establish a nonlinear mapping from control conditions to Gaussian’s deformation, synthesizing motions congruent with both audio content and expressive context.

Video Preprocessing

Audio-Visual Encoder Talking head generation relies on strong correlations between phonemes and orofacial kinematics. While existing audio encoders (*e.g.*, automatic speech recognition (ASR)-focused models) prioritize semantic extraction of speech signals, they fail to capture fine-grained mouth movement features critical for articulatory dynamics. To address this, we adopt SyncTalk’s pre-trained audio-visual encoder (Peng et al. 2024), adversarially trained on the LRS2 dataset (Afouras et al. 2018) with a lip-sync discriminator. This model extracts phoneme-aware mouth movement features a , establishing cross-modal alignment between speech signals and articulatory motion. These features are injected into the deformation field via attention-based modulation, controlling lip-related Gaussian primitive deformations.

Facial Action Encoder Facial expressions during speech production involve complex muscle activations that extend beyond phoneme articulation, including subtle movements such as squinting, eyebrow elevation, and frowning. Current approaches exhibit limitations in modeling these dynamics. For example, some efforts regulate basic blinking patterns (Li et al. 2023; Tang et al. 2022; Liu and Hao 2023) but fail to capture nuanced facial muscle coordination. Blendshape-driven techniques (Peng et al. 2024) enable broader expression control through 3D shape approximations but lack direct correspondence to biomechanical muscle activations. To bridge this gap, we propose a facial action encoder grounded in the Facial Action Coding System (FACS) (Ekman and Friesen 1978). Our framework parameterizes facial dynamics using six anatomically defined Action Units (AUs: 1, 4, 5, 6, 7, 45), selected for two key advantages.

AUs directly map to specific muscle groups (*e.g.*, AU4 for brow lowering, AU6 for cheek elevation) without inducing global facial distortions common to blendshape approaches. In addition, these AUs demonstrate low correlation with phoneme-driven lip movements, enabling independent synchronization of emotional expressions and speech. During training, we extract frame-wise facial expression features $e \in \mathbb{R}^6$ via OpenFace (Baltrusaitis et al. 2018), focusing on AUs governing brow, cheek, and eyelid kinematics. These features are integrated into the deformation field through attention-based modulation, enabling precise control of Gaussian primitives associated with upper-face dynamics.

More Ablation Study

Audio-Visual Encoder. To assess the effectiveness of AVE, we conduct ablation experiments on datasets with constrained head rotations (“Lieu”, “Shaheen” and “Jae-in”), where subtle articulatory dynamics are critical for accurate lip synchronization. Specifically, for AVE-equipped methods (our M2DAO-Talker approach and SyncTalk (Peng et al. 2024)): we replace AVE with DeepSpeech (DS) audio encoding. For DS-based methods (TalkingGaussian (Li et al. 2025)), we substitute DS with AVE encoding. We maintain the identical architectures otherwise for fair comparison, and evaluate their performance across PSNR, LPIPS, and LMD. Experiments in Table 5 demonstrate that AVE implementations outperform DS variants across all metrics, which displays AVE’s advantage in capturing mouth movement dynamics over DS’s semantic speech features. It is speculated that AVE’s focus on articulatory features enhances visual-articulatory alignment. Significantly, our M2DAO-Talker method maintains performance parity with SyncTalk and TalkingGaussian even when using suboptimal DS encoding, demonstrating obvious architectural resilience and superiority.

Backbone	AVE	DS	PSNR \uparrow	LPIPS \downarrow	LMD \downarrow
M2DAO-Talker (Ours)	✓	✓	35.932 35.672	0.0164 0.0167	2.423 2.484
TalkingGaussian (Li et al. 2025)	✓	✓	32.687 32.841	0.0246 0.0242	2.484 2.363
SyncTalk (Peng et al. 2024)	✓	✓	35.075 34.878	0.0178 0.0181	2.503 2.510

Table 7: Results of Audio-Visual Encoder Experiment. We compared the performance of the Audio-Visual Encoder (AVE) and Deepspeech (DS). The best results are indicated in bold.

Backbone	AU	BS	PSNR \uparrow	LPIPS \downarrow	LMD \downarrow
M2DAO-Talker (Ours)	✓	✓	34.475 34.333	0.0229 0.0226	2.636 2.672
TalkingGaussian (Li et al. 2025)	✓	✓	32.042 31.938	0.0319 0.0320	2.712 2.712
SyncTalk (Peng et al. 2024)	✓	✓	33.902 33.905	0.0246 0.0252	2.685 2.660

Table 8: Results of Facial Action Encoder Experiments. We compared the performance of the Action Unit (AU) and Blendshape (BS). The best results are indicated in bold.

Facial Action Encoder. To evaluate the efficacy of FAE, we conduct cross-paradigm ablation experiments by substituting Action Units (AUs) and Blendshapes (BS) across seven datasets with varying expression complexity. For AU-based methods (our M2DAO-Talker approach and TalkingGaussian (Li et al. 2025)), we replace AUs with BS. Conversely, for BS-based methods, we substitute BS with AUs for facial expression control. The performance comparison

across PSNR, LPIPS, and LMD are shown in Table 6, revealing that AU-to-BS substitution causes consistent metric degradation on average (PSNR: -0.142 dB, LMD: $+0.036$). Notably, SyncTalk exhibits atypical behavior: BS substitution improves LPIPS by 2.43% despite minor PSNR/LMD changes. It is supposed that BS’s holistic facial parameterization better aligns with SyncTalk’s motion field paradigm. Overall, AUs outperforms BS in almost scenarios, particularly in complex and diverse expression scenarios (*e.g.*, “May”: $+0.61$ dB, “Obama1” : $+0.29$ dB and “Obama2” : $+0.19$ dB). This validates AUs’ superiority in modeling fine-grained muscle activations critical for subtle expressions.